Available online at www.sciencedirect.com
SCIENCE DIRECT®
Continental Shelf Research 24 (2004) 2297–2316
CONTINENTAL SHELF RESEARCH
www.elsevier.com/locate/csr

Sediment mobility due to currents and waves in the Torres Strait–Gulf of Papua region

M.A. Hemer[a,d,*], P.T. Harris[b,d], R. Coleman[c,d], J. Hunter[d]

[a]*IASOS, University of Tasmania, Private Bag 77, Hobart, TAS 7001, Australia*
[b]*Geoscience Australia, GPO Box 378, Canberra, ACT 2601, Australia*
[c]*School of Geography and Environmental Studies, University of Tasmania, Private Bag 78, Hobart, TAS 7001, Australia*
[d]*Antartic Co-operative Research Centre, Private Bag 80, TAS 7001, Australia*

Available online 11 November 2004

Abstract

The MECO hydrodynamic model (MECO Technical Report No. OMR-118/120, CSIRO Marine Research, 1998) was adapted for the Torres Strait–Gulf of Papua region at 0.05° resolution. Validation of the hydrodynamic model was carried out against observed current meter data and calculated tidal sea levels. Dispersal pathways of sediments derived from the Fly River, and from a resuspension event along the northern Great Barrier Reef were investigated using an Eulerian approach. Sediment input into Torres Strait is found to be greater during the Trade season by approximately 10%. Wave data were also obtained, and together with hydrodynamic model output, sediment mobility due to currents, waves and wave–current interactions was considered for both the Trade and Monsoon seasons. Sediment mobility in the Gulf of Papua is dominated by wave motion, whereas Torres Strait is a mixed environment of waves and tidal currents.

Keywords: Hydrodynamic model; Sediment mobility; Torres Strait

1. Introduction

Torres Strait (hereafter referred to as the Strait) is located at the northern end of the Great Barrier Reef in the northeast of Australia. It forms an oceanographic boundary between two quite separate ocean basins (the Coral Sea/Gulf of Papua and the Gulf of Carpentaria/Arafura Sea). It also defines a biological barrier correlating with the northern limit of the Great Barrier Reef, a political boundary between Australia, Papua New Guinea and Indonesia (West Papua), and a geological mixing zone of terrigenous and calcareous sediments (Harris, 1999). The Strait is an important national, and international, shipping channel, and contains valuable fisheries for prawns and crayfish. Hence, the Strait is considered to be an ocean

*Corresponding author. Now at: Geoscience Australia, GPO Box 378, Canberra, ACT 2601, Australia. Tel.: +61-2-6249-9786; fax: +61-2-6249-9956.
E-mail address: mark.hemer@ga.gov.au (M.A. Hemer).

0278-4343/$ - see front matter © 2004 Published by Elsevier Ltd.
doi:10.1016/j.csr.2004.07.011

region of economic importance to both Australia and Papua New Guinea. The natural environment, however, is being impacted by mining activities in the New Guinea highlands, which input mine tailings into rivers that discharge into the coastal zone. The approval of a gas pipeline to be laid across the Strait also has possible implications for the Torres Strait environment.

The above reasons indicate that knowledge of the Strait's physical and environmental processes is vital to successful management of the region. Harris (1994b) states that sediment transport pathways are of crucial importance to predict impacts which may arise due to increased sediment input to the marine environment from mining and logging operations on the New Guinea landmass. This increased sediment load is capable of smothering corals, or restricting seagrass growth due to sunlight blockage. The transport pathways of sediments are relevant to the fate of many environmentally harmful substances, such as heavy metals, commonly associated with fine sediments.

Harris (1999) identified two key marine geological questions important to the management of the Strait: (i) What are the main dispersal pathways and deposition sites for sediment derived from the Fly River in Torres Strait? (ii) What are the main physical processes controlling sediment erosion, transport and deposition in Torres Strait? These questions were addressed from available current meter, surficial sediment distributions, seismic survey and coring data on terrigenous sediment input and dispersal in Torres Strait. The aims of this paper are to address these same questions with the use of a 3-D hydrodynamic model, with wave and current modules, and to investigate seasonally dominant sediment transport mechanisms in the region.

2. Background

2.1. Topography

The area studied, shown in Fig. 1, includes the waters of the northern Great Barrier Reef (GBR) continental shelf and the Gulf of Papua along with the north-eastern section of the Gulf of Carpentaria. Numerous islands, coral reefs and shoals form a complex bathymetry. The shelf is separated from the Coral Sea by a string of reefs forming the outer GBR. The GBR continental shelf is then open to the Gulf of Papua by the Great North East Channel, and the Gulf of Carpentaria by Torres Strait. The Strait is approximately 100 km long in the north–south direction and 20–60 km wide east–west. The bathymetry of the main shipping channels within the Strait itself have been well charted and indicate a shallow seabed, with depths generally in the range of 6–9 m, with channels up to 12 m depth (Harris, 1994b). However, there remain large regions of the Strait where bathymetric data are sparse. The 'Torres Strait Islands' extend north-northwestwards from Cape York, where fringing coral reefs with an East–West elongation have grown. The waters west of the Strait are shallow, shoaling westward, with the 20 m isobath 75 km to the west in the Gulf of Carpentaria.

To the north of the Great North East Channel, positioned on the south coast of Papua New Guinea, the Fly River Delta is a funnel-shaped, highly dynamic, macrotidal deltaic system (Harris et al., 1993). Within the delta, strong tidal currents and superimposed surface swell waves cause continuous reworking of sediments such that the turbidity of estuarine water is commonly greater than the incoming river water. The high tidal and wave energy input, along with a river sediment input of 125×10^6 tonnes a^{-1},[1] result in 'fluid muds' which have been observed near the bottom with suspended sediment concentrations of up to 40 g L^{-1} (Wolanski and Eagle, 1991).

2.2. Winds

Seasonal variations in the annual wind field with an almost complete reversal of direction are well known. During the southern hemisphere winter (April–November), the south-easterly (SE) trade winds dominate, and in the summer (December–

[1]Sediment load after Ok Tedi gold and copper mine was opened. Before European settlement, the sediment load of the Fly River system was 85×10^6 tonnes a^{-1} (Harris et al., 1993).

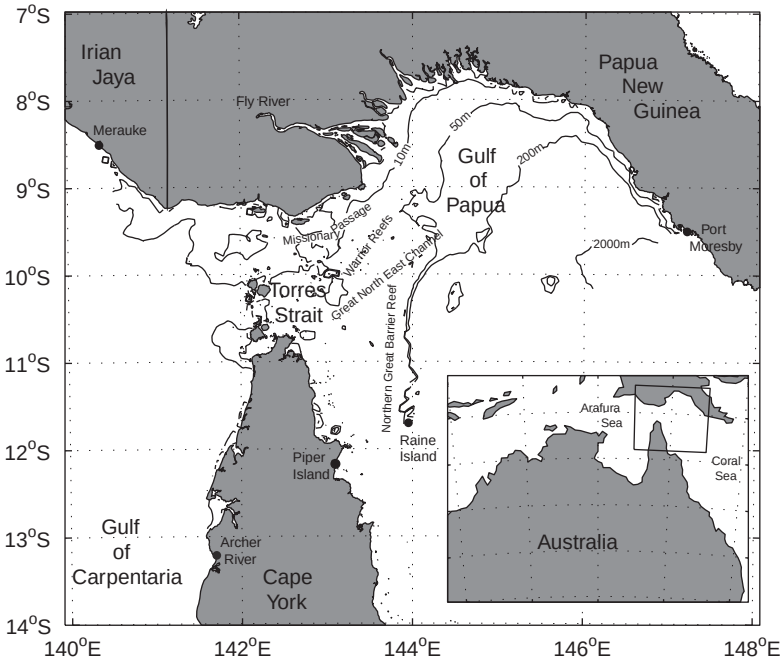

Fig. 1. Torres Strait and Gulf of Papua bathymetry and locality.

March), the northerly monsoon takes over. Wolanski and Thomson (1984) found the monsoon to have alternating easterly and westerly components in the region. Typical wind speeds in the area are of order 1–2 m s^{-1} during the monsoon season, and ~5 m s^{-1} during the trade season.

2.3. Waves

During the SE trades, Torres Strait is generally protected from surface waves generated in the Coral Sea by the northern-most extension of the GBR, serving to block long-period swell. As a result, only locally generated waves are found on the GBR shelf. In contrast however, the Fly River Delta remains exposed to Coral Sea generated swell. During the NW monsoon, offshore winds result in little or no long-period swell propagating towards the south coast of PNG. Satellite data indicate that significant wave height (SWH) rarely, if ever, exceeds 3.5 m in Torres Strait, and is nearly always less than 1.5 m during the NW monsoon (McMillan, 1982). Fig. 2 shows SWHs averaged seasonally for a year using Bureau of Meteorology WAM data.

2.4. Physical oceanography

Tides within Torres Strait are characterised by strong tidal currents and rapid spatial changes in tidal elevations. Tidal ranges are of the order of 3 m. Torres Strait forms the intersection of two separate and dissimilar tidal regimes of the Gulf of Papua/Coral Sea and the Gulf of Carpentaria/Arafura Sea, both dominated by the M_2 constituent (Amin, 1978). The two domains are out of phase with each other (variations in phase of the M_2 constituent of ~180° through the strait proper are observed) and show little correlation in the tidal records either side of the Strait (Bode and Mason, 1994). As a result of the tides being incoherent on either side of the Strait, large pressure gradients are experienced through the Strait and these drive strong tidal currents magnified by flow channelisation in passages amongst dense coral reefs through the Strait. The incoherency also indicates that the tidal waves are

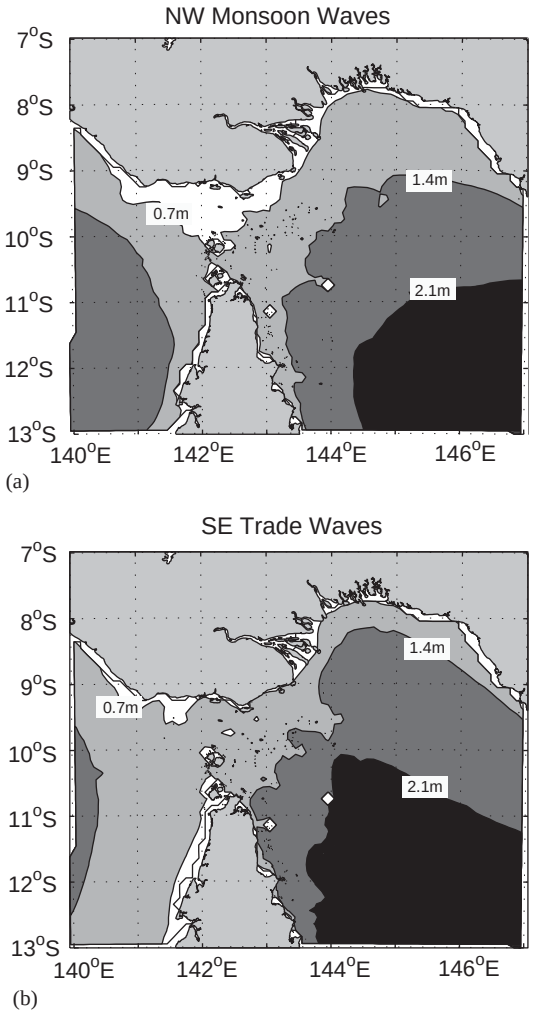

Fig. 2. Seasonally averaged significant wave heights (m) for a given year (1998) of Bureau of Meteorology WAM results for (a) NW monsoon and (b) SE trades.

unable to propagate completely across the Strait, with only about 30% of the tidal wave transmitted from basin to basin; the rest is dissipated through friction (Wolanski et al., 1988). This large tidal energy dissipation leads to tidal current scour and sediment reworking (Harris and Baker, 1991). Dense coral reefs further complicate the tidal dynamics.

A number of non-tidal sea-level oscillations exist within the area. These include (i) 50 cm amplitude sea-level oscillations in the Gulf of Carpentaria driven by cyclones in the Arafura Sea (Melville and Buchwald, 1976), (ii) surges generated on either side of the Strait (Amin, 1978), (iii) large low-frequency sea-level oscillations on the northern GBR shelf (highly coherent on the shelf) that are about 30 cm peak to trough (Wolanski and Thomson, 1984), and (iv) monthly mean sea levels (Wolanski, 1986). All of these have been concluded to be incoherent on either side of the Strait, so it is expected that at all time scales there is little propagation through Torres Strait.

Within the Strait, the low-frequency (mainly wind-driven) component of the current is significantly weaker than the tidal component. Over a sampling period of 2 months, the low-frequency currents were observed to reverse direction several times with mean speeds always less than $0.1\,\mathrm{m\,s^{-1}}$ (Wolanski et al., 1988). Wind-driven currents are observed to reverse in sign seasonally, with flow being generally westwards during the SE trades season (April–November) and eastwards during the NW monsoon (December–March) (Harris, 1994b). Wolanski et al. (1988) found that baroclinic motions within the Strait are negligible due to the high-energy shallow waters of the region.

There are three basic vertical structures of water properties in the region of interest (Wolanski, 1986). The first one is found within the Strait and the northern GBR shelf where tidal mixing is large and the water has well-mixed properties of temperature and salinity. The second type is found in the inshore waters of the Gulf of Papua and is characterised by stepped salinity and temperature profiles resulting from river runoff. The third type is found in the Coral Sea and is characterised by a stepped temperature profile and a fairly uniform vertical profile of salinity.

2.5. *Surficial sediments*

The nature of the surficial sediments varies as a function of both the vicinity of river sediment sources (i.e. the Fly River) and the tidal current regime (Harris, 1999). In the regions where tidal currents attain a local maximum (maximum bottom stress), the seabed is scoured clear of unconsolidated sediments, leaving behind a lag

gravel or limestone pavement (exposed bedrock). With increasing distance from the channels, sediment of decreasing grain size is deposited. Away from the scoured zone, sand/gravel ribbons give way to dunes, and at greater distance from reef passages, current strengths are low enough to allow fine silt and clay-sized particles to settle (Harris, 1994a).

Grain size distribution and percentage content of calcium carbonate are the two most useful descriptors of surficial sediment in the area. A high carbonate content indicates sediment derived from benthic foraminifers, bryozoans, molluscs, alga *Halimede* and small amounts of coral (Harris, 1988). The Fly River Delta is characterised by sediments of low carbonate content (terrigenous sediments) whereas the sediments within Torres Strait generally have a high carbonate content in excess of 80% (Harris, 1988). An effective measure of grain size distribution is mud content, defined as the percentage by dry weight of grains less than 63 μm (Harris, 1999), and relates relative current energy to the relative position of the sediment along the transport path, from source to depositional environments. Harris (1988) mapped the surficial sediments of Torres Strait displaying mud content. This shows two regions of high mud content: one forms a belt of $>80\%$ mud across the front of the Fly River Delta, the other ($>60\%$ mud) in the eastern section of Torres Strait between the numerous reefs. Both of these regions are low-energy depositional areas (Harris, 1999). Regions of low mud content represent regions of mainly sand and gravel. These more winnowed areas, where mud content is less than 10%, are associated with bedforms.

2.6. Sediment transport

2.6.1. Bedload

Tidally influenced bedload is characterised by bedload partings (BLPs), where tidally averaged bedload transport vectors diverge from zones of maximum bottom stress (Stride, 1982). Such areas are characterised by surficial sediments that have been winnowed to lag gravel (armoured beds) or, in extreme cases, exposed bedrock. With increased distance from the BLP, the process changes from erosion to transport forming mobile sand deposits (dunes and ribbons) (Johnson et al., 1982). Between these two zones of scour and deposition, regions of areally extensive bedforms occur. These bedforms indicate that in these regions also, the bed sediments are regularly mobilised, and that the associated surficial sediments comprise well-sorted sands and gravels (Harris, 1999). Sandwaves (subtidal dunes) of 4–5 m height are observed to reverse asymmetry and migration direction with the seasonal changes in current direction (Harris, 1989).

Sand and mud distributions are affected by the combined action of tidal and wind-driven currents, producing areas of migrating bedforms, in which soft, sand-size carbonate grains are reworked and broken down into silt-size particles for removal, in suspension, away from tidal scour zones to high carbonate sediment depocentres located in eastern and central Torres Strait (Harris, 1994b). Tidal currents in combination with wind-generated waves give rise to a turbidity maximum in central Torres Strait (Harris and Baker, 1991).

2.6.2. Suspended load

Harris (1999) indicates that the highest concentrations of suspended sediment occur in constricted passages between reefs. Measurements during the trade wind season (September) showed higher SSC associated with the Fly Delta and the southern coast of PNG. Similar concentrations are observed elsewhere in the region with the mean surface SSC of $9.14\,\mathrm{mg\,L^{-1}}$ in the NW monsoon, and a mean SSC of $5.4\,\mathrm{mg\,L^{-1}}$ during the SE trades at all stations (excluding the Fly Delta stations).

The direction of residual (tidally averaged) flow predominately determines the path of a suspended sediment particle in Torres Strait (Harris, 1999). Turbidity measurements from Missionary Passage indicate that during spring tides, SSC are higher ($20–30\,\mathrm{mg\,L^{-1}}$) than on neaps ($<10\,\mathrm{mg\,L^{-1}}$). For both spring and neap tides, high SSC coincide with periods of high current speed. The passage north of Saibai Island displayed similar features. Harris (1999) found that for both of these regions, the net suspended sediment transport was mostly towards the west (flood-dominated). Hence, it may be

concluded that the westward flowing wind-driven residual current, which dominates Torres Strait during the SE trades, controls the local westward transport of suspended sediments along the southern coast of PNG between Daru and Saibai Island.

At the Fly River Delta front, surface waves generated by the SE trades rework muds and sands to winnow out the fine-grained sediments. During the NW monsoon, minimal surface wave activity results in the deposition of mud drape, resulting in seasonal sand–mud interbeds (varves) (Harris et al., 1993).

The Fly is one of the largest rivers in the world in terms of annual sediment load (125×10^6 tonnes a^{-1}) (Harris et al., 1993) and has a tidal range greater than 3 m, indicating a tidally dominated delta (in contrast to deltas which may also be dominated by surface waves or river input). Approximately 238 $km^3 a^{-1}$ of water is discharged from the Fly (Alongi et al., 1992), with most of the sediment load provided from mountain areas as a result of land slides triggered by tectonic events. Deforestation and mining in the catchment have further increased the sediment load.

Harris et al. (1993) estimated a sediment budget for the Fly River based on the sediment load prior to the opening of the Ok Tedi gold and copper mine. Before the mine opened, 85×10^6 tonnes of sediment (90% suspended load, 10% bedload) was discharged from the Fly annually. About half of this (47×10^6 tonnes) is estimated to be deposited within the Fly delta. Sands are deposited in the upper estuary, and muds deposited further offshore in the pro-deltaic environment. The remaining sediments are dispersed over the shelf regions. Harris et al. (1993) postulated that density-driven currents could transport 'fluid muds' eastwards onto the shelf across isobaths and possibly into the Coral Sea basin following submarine drainage channels. Wind-driven currents are thought to transport 40% of the annual Fly discharge in suspension north-eastwards into the Gulf of Papua, and a further 5% westwards along the south coast of Papua New Guinea. Less than 2% of the Fly sediments are thought to be deposited in Torres Strait to the south (Harris et al., 1993).

The amount of sediment not accounted for in the budget may follow a number of paths: (i) sediment retained and deposited in the deltaic channels; (ii) transported offshore for deposition in the Gulf of Papua; (iii) transported westwards along the south coast of Papua New Guinea; (iv) transported southwards into Torres Strait; and (v) some combination of the above—the more likely result. The aim of this study is to identify which of these paths are a more likely combination.

3. Model description

The Model for Estuaries and Coastal Oceans (MECO) model used for the study is a 3D, non-linear, variable density, hydrodynamic model (Walker and Waring, 1998). It provides 3D distributions of salinity, temperature, velocity and concentrations of passive tracers, given input fluxes of water, salt, heat and passive tracers, and forcing by winds, atmospheric pressure gradients and sea-level variations. MECO is based on the equations described by Blumberg and Herring (1987) using a z-grid in the vertical and an Arakawa C-grid in curvilinear horizontal coordinates (see, for example, Mesinger and Arakawa, 1976). The model is described in detail (Walker and Waring, 1998; Walker and Fandry, 1993) and validated in a number of studies (Walker and Fandry, 1993; Walker, 1996, 1999; Andrewartha and Walker, 1997, 1999). MECO, being a z-layer model, has implemented a scheme of variable bottom layer thickness so that the bathymetry may be better resolved, removing the step-like features at the bottom as observed in other z-layer models. Momentum is transferred vertically within the water column by turbulent mixing, represented in the model using an eddy viscosity parameterisation as described by Bowden and Hamilton (1975).

The model grid encompasses all of Torres Strait and the Fly River Delta—plus most of the Gulf of Papua and a region of the Gulf of Carpentaria—to allow good representation of flow through Torres Strait. It was preferred that the open boundaries were bounded by existing ports in order that tide, sea level and meteorological data would be readily available at these points. As a result, the main grid (Fig. 3) was chosen such that the western boundary was defined by Merauke, Irian Jaya

(8°31.8′S, 140°20′E) in the north, and Archer River, Qld, Australia (13°20′S, 141°39′E) in the south. The eastern boundary was defined by Piper Island (12°15′S, 143°15′E), Raine Island (11°36′S, 144°3′E) and Port Moresby, Papua New Guinea (8°30′S, 148°47′E). The grid was at an azimuth of 40°. The horizontal resolution of the model grid is 0.05°. Vertically, the model has 22 z-layer interfaces to accommodate uniform 3 m spacing from the surface to the 30 m isobath (covering the dominant portion of Torres Strait) and then parabolic spacing up to the 3000 m maximum depth. The model uses an explicit, forward, mode-split time-stepping scheme, with an external time step of 10 s and an internal time step of 100 s, to maintain model stability.

Digital bathymetry data were obtained by smoothing the AGSO bathymetric 30 s grid of the Australian region (Porter-Smith, 2000), and for the North of 8.5°S, from ETOPO5 5 min lat–lon grid (NOAA, 1988). Depths were truncated to lie between a minimum of 7 m and a maximum of 3000 m to avoid problems with wetting and drying of coastal zones given large tidal ranges. Manual smoothing of bathymetry was required in three regions to alleviate instabilities which occurred during some model runs. These areas included (i) the steep shelf off the coastline of PNG, nearby Port Moresby, (ii) the steep shelf to the north of Raine Island, and (iii) the shallow waters between the western boundary and the eastern coast of the Gulf of Carpentaria. A contour plot of the final model bathymetry is shown in Fig. 1. Digital coastline data were obtained from the Global Self-consistent Hierarchial High-resolution Shoreline (GSHHS, Wessell and Smith, 1996) at a tolerance of 200 m.

The western and eastern open boundaries of the model were tidally forced. Surface elevations were calculated using harmonic constants for nine tidal constituents (M_2, S_2, K_1, O_1, N_2, Q_1, Sa, Ssa, Msf) obtained from the Admiralty data set (Flater,

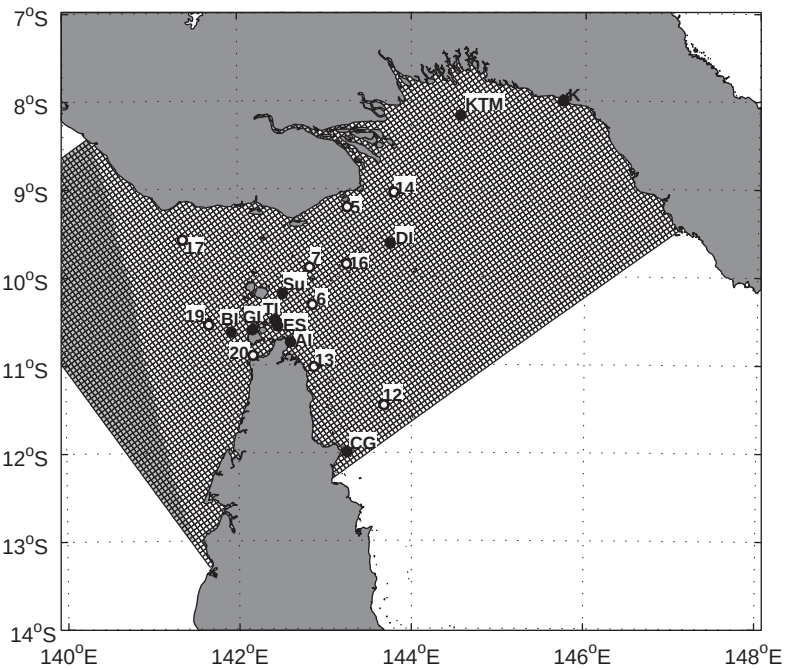

Fig. 3. Location diagram for Torres Strait–Gulf of Papua model grid and tide gauge locations. AI, Albany Island; BI, Booby Island; CG, Cape Grenville; DI, Darnley Island; ES, East Strait Island; GI, Goods Island; K, Kerema; KTM, Kumul Tkr Mrg; Su, Suarji Island; andTI, Tern Island. Current meter positions 5, 6, 7, 12, 13, 14, 16, 17, 19 and 20 are also shown. Dark shaded squares are outside the model domain.

1999). Points on the western boundary were forced by interpolating elevation time series calculated at Archer River and Merauke using a $1/r$ nearest-neighbour interpolation. Points on the eastern open boundary between the Australian mainland and Raine Island (in the Coral Sea) were forced by interpolating elevations calculated at Piper Island and Raine Island. The remaining boundary, northeast of Raine Island, was forced by interpolating data between Raine Island and Port Moresby. The model was generally run for a period of 90 days. This allowed harmonic analysis to easily obtain estimates of the main five tidal constituents (M_2, S_2, K_1, O_1 and N_2).

Atmospheric pressure and wind speed were obtained by interpolating the six-hourly NCEP–NCAR database onto the model grid (Kalnay et al., 1996). The formulation of Large and Pond (1981) was used to calculate the wind stress as input to the model at each model time step.

The temperature and salinity fields were specified by a temporally uniform density field designated from the mean Climatology of Australian Regional Seas (CARS) (Ridgway et al., 2000). Temperature and salinity are influenced by advective and diffusive processes in the model. The model configuration used has no surface heat input, significant lack of freshwater inflows into the Gulf of Papua, and no evaporation. Without such forcing, the thermohaline field will become unrealistic. This is overcome by 'relaxing' the field towards the climatological values. The relaxation follows an exponential decay at a rate specified by a time constant set at 20 days and is calculated every 5 h. In each model run, the relaxation was towards a temporally uniform 3D field sourced from CARS.

A series of preliminary model runs were completed that were forced using 90-day time series of wind and tides, and CARS temperature and salinity fields. Results showed that wind and tidal forcing dominated circulation, and that baroclinic forcing impacted currents by only 6%.

To provide a long-term pressure gradient, low-frequency sea-level information is specified for each of the open boundaries. This was specified in the form of dynamic height calculated from the CARS temperature and salinity climatology described above. A reference level of no motion at 500 m was assumed.

The outflow of the Fly River ($238\,km^3\,a^{-1}$, Alongi et al., 1992) was specified by an open boundary of one cell width with a velocity of $0.2\,m\,s^{-1}$ providing an addition of momentum to the model, and freshwater, with a forcing salinity of 12 psu specified.

Twelve months of predicted swell data has been obtained from the Bureau of Meteorology WAM runs for the period of 01/01/1997 to 31/12/1997 (Greenslade, 2001). These data are provided on a 0.5° grid at six hourly intervals, and includes SWH (H_s), mean wave period (T_m) and mean wave direction (ϕ_m). From these parametres, bottom wave orbital velocities can be estimated. The time period of obtained wave data did not correspond to the period of field observations; however, they were assumed to be representative of the seasonal wave variation.

Bottom friction calculations within the model are determined using the quadratic law described in Walker and Fandry (1993). This involves the choice of a typical bottom roughness length scale $z_0 = 0.002$ m, and a minimum drag coefficient, $C_{dmin} = 0.0033$. These values are typical of those taken from the literature (e.g. Jonsson, 1966). Both our calculations and those of Andrewartha and Walker (1999) show that the choice of these parameters is insensitive to output values. The use of wave-enhanced bottom friction calculations were included on later runs (see Section 6.3) to better represent the enhanced bottom friction in the near-shore zone.

The background mixing constants V_{zo} and K_{zo} were set to the value of 0.0005 and $0.00025\,m^2\,s^{-1}$, respectively (Bowden and Hamilton, 1975). Values for the eddy diffusivity coefficient, α_V, and the tracer diffusivity coefficient, α_K, were set at 0.0625 and 0.03, respectively (Csanady, 1982). These diffusivity values were found to significantly alter currents and sea surface levels throughout the model domain, and were tuned to minimise the standard error to the available in situ data. Horizontal diffusion of momentum with a minimal diffusivity of $10.0\,m^2\,s^{-1}$ was added to ensure model stability.

4. Model validation

4.1. Tidal elevations

A harmonic analysis was performed of the modelled sea-level data at 10 sites in the model domain (Fig. 3), and compared to values given in the ANTT (Table 1). A regression analysis between modelled and calculated sea-level data was also performed.

Fig. 4 overlays modelled sea levels with observed sea levels at four sites within the model domain. Tern Island (TI) and Darnley Island (DI) show a slight phase lag (approximately 65° at DI); however, amplitudes correspond well at each of the four sites. The largest discrepancies are observed at Booby Island and Goods Island (Table 2) with R values of 0.6620 and 0.6567, respectively. The M_2 amplitude and phase errors at these two points are 18 cm, 31 cm, 60° and 63°, respectively. Note that these two sites lie within the Strait where rapid changes in tidal amplitude and phase are observed. At other sites, values of R are greater than 0.87 with amplitude errors generally less than 5 cm.

4.2. Current data

Measured current data within the model domain, with records in excess of 30 days, have been obtained for two intervals: (i) three sites (stations 5, 6, 7) during the period of February–April 1990; and (ii) seven sites (stations 12, 13, 14, 16, 17, 19, 20) during the period of January–March 1993 (Harris, 1994b) (Fig. 3). Possible errors exist in the current meter data. Many of the current meters had problems of marine fouling (Harris, 1993), capable of reducing the observed current signal.

Regression statistics for modelled vs. observed currents at all stations are listed in Table 2. The model generally does quite well at stations 5, 13, 14, 16, 19 and 20, with R^2 values ranging from 0.3 to 0.7 and slopes ranging from 0.3 to 1.8. As an example, plots of the comparitive analyses between modelled and observed currents at station 16 are shown (Fig. 5).

Hydrodynamic model performance for currents in stations 6, 7, 12 and 17 is poorer, with R^2 values ranging from near zero to 0.2. It is evident that processes within the Strait are poorly represented in the model, and the most likely candidates are rapid changes in tidal constituents across the Strait that are due to complex topography not being represented in the bathymetric model. Previous modelling of the tidal current regime of the region (Bode and Mason, 1994) consisted of an involved sub-grid scale parameterisation of reef porosities.

5. Sediment transport studies

5.1. Steady current-induced bed shear stresses and bedload transport pathways

Bottom currents were output from the model, taken as the currents at 3.5 m above the seafloor. Maximum current-induced bed shear stress vectors were computed from the maximum current from each grid point during each model run, and averaged for each season from the 90-day model runs. NW monsoon seasonal averages were taken from five 90-day model runs, each beginning on the 1st January for years 1990–1994 inclusive, and the SE trades seasonal averages from five 90-day model runs, beginning on the 1st of April for years 1990–1994 inclusive. Maps of seasonally averaged maximum current-induced bed shear stress vectors are displayed in Fig. 6.

During the NW monsoon (Fig. 6a) regions of maximum bed shear stress coincide closely with those predicted by Harris (1994b) from the facies model in areas between the Warrior Reefs, and in passages amongst the Torres Strait Islands. An additional region of high-bed shear stress is found along the northern extent of the Great Barrier Reef where bed stress magnitudes are as large as $3\,\mathrm{N\,m^{-2}}$. The maximum bed stress vectors indicate regions of BLP diverging from a region of maximum bed shear stress (in western Torres Strait, and between the Torres Strait Island and Warrior Reefs). However, throughout the region, a westward trend is observed.

The maximum bed shear stress during the trades (Fig. 6b) indicates a very similar situation to the monsoon. One zone observed to have changed direction seasonally is the Adolphus Channel at

Table 1
Observed and modelled tidal harmonic constituents for Torres Strait points

Site		M_2	S_2	N_2	K_1	O_1	s.d.	m	R
AI	Observed	0.5954	0.5124	0.2095	0.4657	0.2145			
		8.06	32.20	25.90	151.69	204.47	0.1511	0.9800	0.9752
	Modelled	0.6407	0.4856	0.2278	0.3988	0.2128			
		17.97	22.07	28.30	162.28	221.54			
BI	Observed	0.7160	0.1410	0.1680	0.6890	0.4260			
		229.60	98.20	276.00	166.50	228.80	0.6382	0.6569	0.6620
	Modelled	0.8972	0.1538	0.1951	0.4850	0.2827			
		169.51	8.57	230.37	167.70	228.37			
CG	Observed	0.6287	0.4733	0.1798	0.2960	0.1590			
		57.00	102.13	67.63	175.19	204.87	0.1605	0.9579	0.9670
	Modelled	0.6472	0.4141	0.2196	0.3363	0.1656			
		40.15	100.30	46.11	182.58	204.73			
DI	Observed	0.7112	0.4239	0.2837	0.3677	0.1780			
		80.98	125.56	102.89	190.24	216.63	0.3590	0.8218	0.8722
	Modelled	0.7601	0.5027	0.2618	0.3392	0.1710			
		11.71	169.22	122.98	222.38	235.28			
ES	Observed	0.4714	0.5254	0.2484	0.4949	0.2505			
		345.49	24.80	0.76	149.72	206.99	0.2497	0.9197	0.9289
	Modelled	0.6648	0.3901	0.2220	0.4189	0.2286			
		364.00	20.65	4.25	161.18	225.13			
GI	Observed	0.5290	0.2030	0.1360	0.6730	0.3970			
		228.50	59.40	284.50	160.30	223.10	0.5840	0.6153	0.6567
	Modelled	0.8314	0.0846	0.2058	0.4727	0.2641			
		165.36	31.29	241.37	166.12	229.69			
K	Observed	0.5500	0.3300	0.1700	0.2900	0.1400			
		68.00	102.00	92.00	161.00	205.00	0.1352	0.9002	0.9720
	Modelled	0.5997	0.3603	0.2038	0.2872	0.1452			
		52.60	91.04	76.88	153.57	201.93			
KTM	Observed	0.7560	0.3950	0.2100	0.3400	0.1400			
		0.6270	89.00	95.20	169.50	204.50	0.1723	0.9095	0.9718
	Modelled	0.7877	0.4813	0.2640	0.3093	0.1526			
		49.28	74.06	90.39	172.41	202.89			
Su	Observed	0.5454	0.5636	0.1793	0.4994	0.2109			
		348.52	16.41	12.68	147.56	179.68	0.2875	0.9929	0.9081
	Modelled	0.5639	0.4112	0.2018	0.4275	0.2350			
		379.58	11.89	36.60	164.29	177.42			
TI	Observed	0.5040	0.5030	0.1960	0.5010	0.2340			
		347.08	22.03	6.30	150.29	205.42	0.2654	0.8968	0.9192
	Modelled	0.6708	0.3808	0.2223	0.4211	0.2297			
		370.61	16.96	18.40	162.79	222.02			

Amplitudes (first row) are in metres, Phase (second row) in degrees relative to GMT. Sites are displayed in Fig. 5. s.d.—standard deviation, m—slope of scatter plot correlation line ($m<1$ indicates model overestimates observed sea-level), R—correlation coefficient between observed and modelled time series.

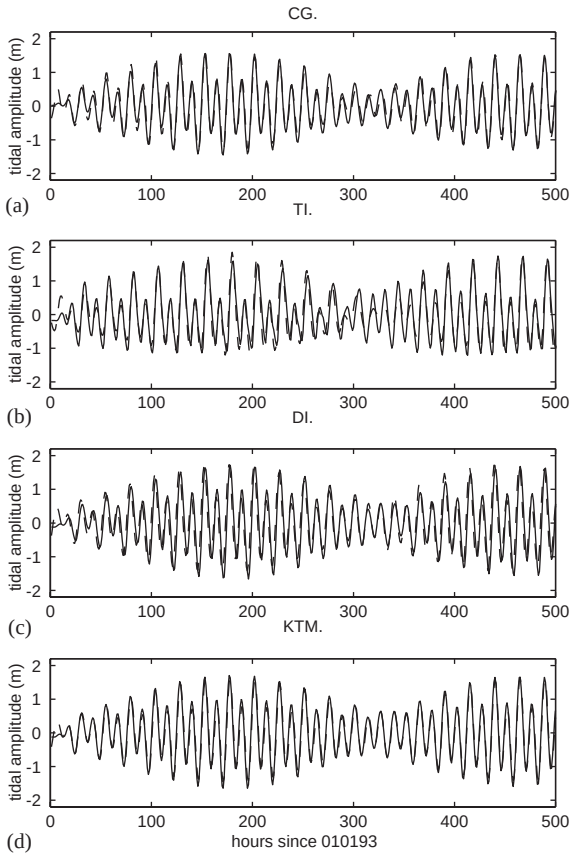

Fig. 4. Modelled (dashed) and observed (solid) sea level at four locations in the model domain from 1993 model runs (hours since 1 January 1993). (a) Cape Grenville (CG), (b) Tern Island (TI), (c) Darnley Island (DI), and (d) Kumul Tkr Mrg (KTM).

the northern tip of Cape York. This seasonal reversal has been previously observed from reversing bedform direction (Harris, 1989). The other main area is in the shallow waters to the west of Cape York. The greatest seasonal variation is observed at the far east of the model domain, adjacent to Port Moresby. These large vectors are likely to be a result of direct boundary forcing, magnified due to the narrow shelf in the area. However, the seasonal dependence is probable. The strong persistent westward bed stress vectors to the northwest of the Strait reflect the large sandwaves observed in this area by Harris (1991). Areas of decreasing bed stress magnitude suggest sediment depocentres, and the location of these correspond to those listed by Harris (1988) as (1) the Endeavour Strait tidal delta, (2) the Turnagain Island region, and (3) a small area in the Eastern Patch Reefs is suggested.

Maximum stress magnitudes and directions differ only slightly between the trade and monsoon seasons. Shelf bottom stress magnitudes of approximately $2\,\mathrm{N\,m^{-2}}$ are observed during each season. The similarities between seasons suggest that maximum bottom stress vectors are a result of tidal forcing, and not the prevailing wind conditions.

5.2. Tracer studies of sediment transport

Ocean currents and sediment dispersal were simulated for 90 days from the 1st of January

Table 2
Linear regression slope and R^2 values for modelled vs. observed low-pass filtered currents

Site	Water depth (m)	Meter height (m)	n	Slope	R^2
Stn 5	7	31	6802	1.60 (0.14)	0.64 (0.44)
Stn 6	25	4	4153	1.15 (0.60)	0.09 (0.07)
Stn 7	26	7	5659	0.03 (0.23)	0.17 (0.05)
Stn 12	31	10	5174	0.29 (1.21)	0.18 (0.48)
Stn 13	27	5	5173	0.79 (1.80)	0.66 (0.24)
Stn 14	24	4	5013	0.15 (1.58)	0.44 (0.45)
Stn 16	31	6	5000	0.46 (1.60)	0.49 (0.56)
Stn 17	19	4	4790	0.37 (0.067)	0.012 (0.09)
Stn 19	23	6	4790	0.24 (0.84)	0.50 (0.37)
Stn 20	16	5	4871	0.08 (1.72)	0.24 (0.66)

Values quoted for east component and north component (in brackets).

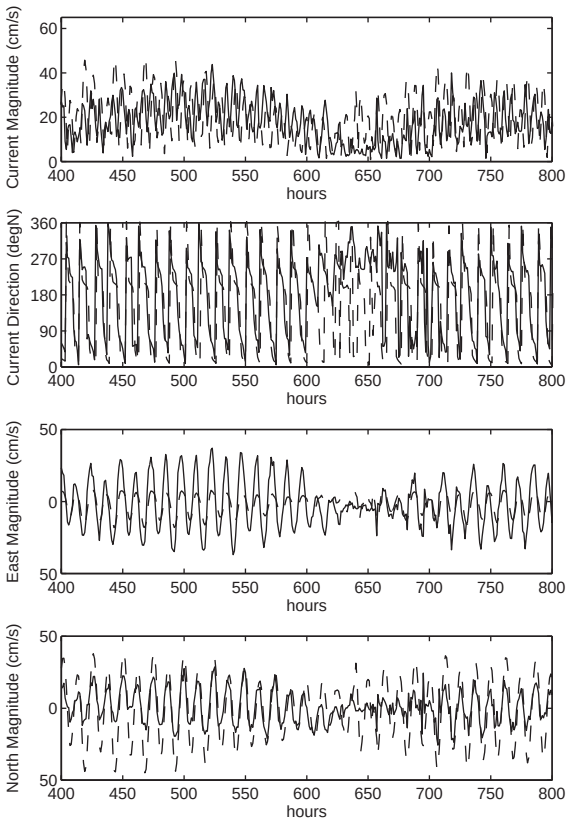

Fig. 5. Modelled (dashed) and observed (solid) currents from station 16, February 1993.

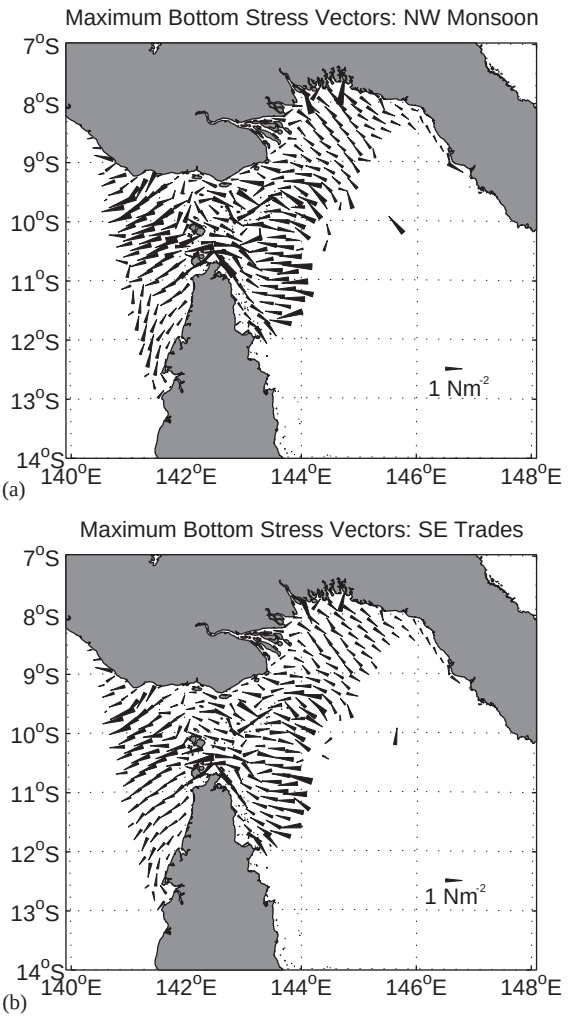

Fig. 6. Maximum bottom stress vectors indicating bedload transport pathways on the Continental Shelf (depth < 300 m) (a) monsoon and (b) trades. Dominant pathways correspond with those indicated by Harris (1988).

(representing the monsoon), and for 90 days from the 1st of April (representing the trades) for years 1990–1994 and averaged. The model parameters chosen for these simulations were the same as for the model-observation runs described above. These runs allow for comparisons of sediment transport pathways on a seasonal basis. Sediment was input at two places, one to represent the Northern Great Barrier Reef (NGBR) and one to represent the Fly River.

The regions of maximum current-induced shear stress along the NGBR suggest that this may be a region of high sediment resuspension. As a result, model runs were performed to simulate the dispersal pathways of suspended calcareous muds derived from the breakdown of clastic carbonates along the NGBR and the accumulation/deposition zones resulting from a resuspension event in the region. Sediment was introduced into the model at position 9°30′S, 144°15′E at a height of 1 m above the seafloor to represent suspended sediment. The sediment was introduced 2 days after the start of the run to avoid model starting transients, and was continuous thereafter. The sediment for this application was assumed to have a settling velocity of $0.0005\,\mathrm{m\,s^{-1}}$ representing a medium silt (Dyer, 1986). Sediment was added at a constant rate of $1\,\mathrm{m^3\,s^{-1}}$, equivalent to an erosion rate of O ($1\,\mathrm{mm\,day^{-1}}$), at a concentration of $0.1\,\mathrm{g\,L^{-1}}$

representing a source of suspended calcareous sediment mobilised on the NGBR.

To simulate the dispersal of suspended terrigenous sediments derived from the Fly River, suspended sediments were introduced into the model at two locations within the Fly River Delta: one at position 8°45′S, 143°30′E, and the other at 8°15′S, 143°30′E at a height of 1 m above the seafloor (Fig. 7). The sediment was introduced to the model 2 days after the start of each run to avoid model starting transients, and was continuous thereafter. The sediment was assumed to be a coarse silt, with settling velocity w_s equal to $-0.00081\,\mathrm{m\,s^{-1}}$. Sediment was added at a rate of $1000\,\mathrm{m^3\,s^{-1}}$ at a concentration of $0.5\,\mathrm{g\,L^{-1}}$ representing a source of suspended sediment of typical suspended sediment concentrations from the Fly River Delta.

Contour plots of the averaged modelled depth-integrated suspended sediment concentrations for

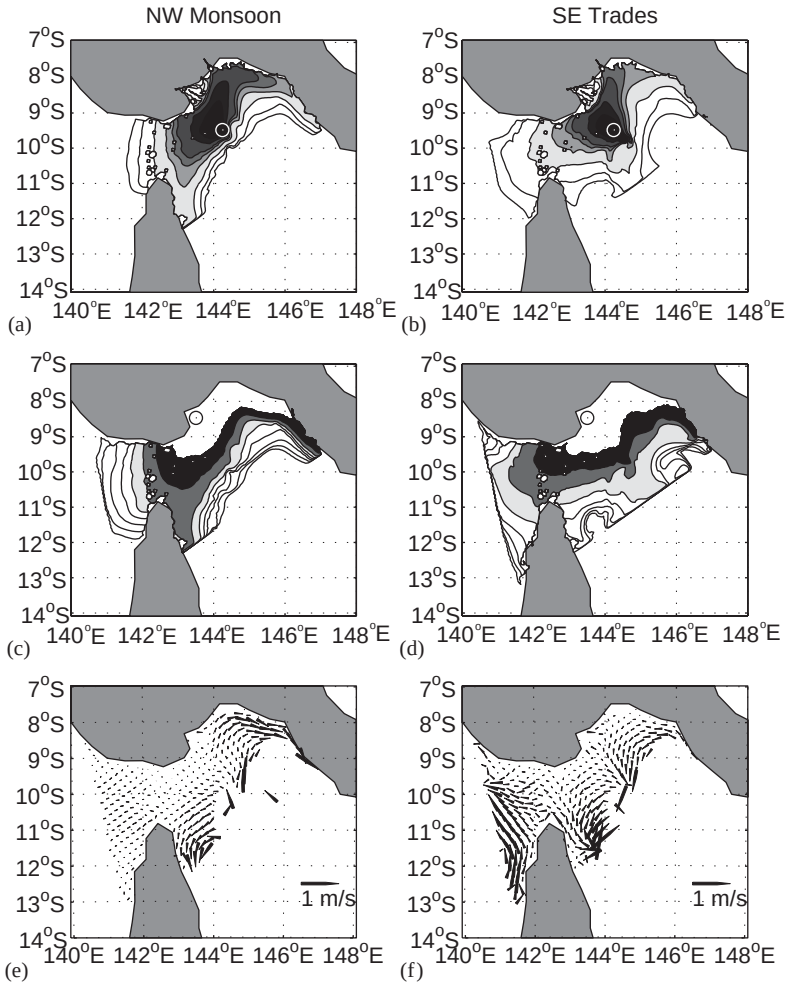

Fig. 7. Modelled plumes, with mean depth-integrated currents after 90 days, averaged from 1990–1994. Resultant plume from resuspension event on the Northern Great Barrier Reef during (a) monsoon season and (b) trades season; resultant plume from Fly River suspended sediment for (c) monsoon season and (d) trades season; mean depth-integrated currents (e and f) for (e) monsoon season, and (f) trades season. (○ marks position of introduced tracer. Monsoon tracers introduced on 1 January of each year; trades tracers introduced on 1 April of each model year.) Contours in plume plots are fractions of initial concentration 1, 0.01, 0.001 and decrease in order of magnitude onwards.

periods of 90 days after the sediment was initially introduced for the NGBR and Fly River plumes, and mean depth averaged currents are shown in Fig. 8. The model allows the sediment to leave the model grid by settling and/or lateral transport; however, no resuspension mechanism is included in the model.

The NGBR sediment plume indicates a reverse in direction seasonally as found by Wolanski et al. (1988) and suggested from bedforms (Harris, 1989). Monsoon conditions lead to a large component of sediment moving north-eastwards, along the south coast of PNG. The suspended sediment plume is also observed to travel southwards past the eastern edge of Cape York, inside the NGBR. SE trade conditions lead to a greater component of the plume moving directly offshore to be deposited in

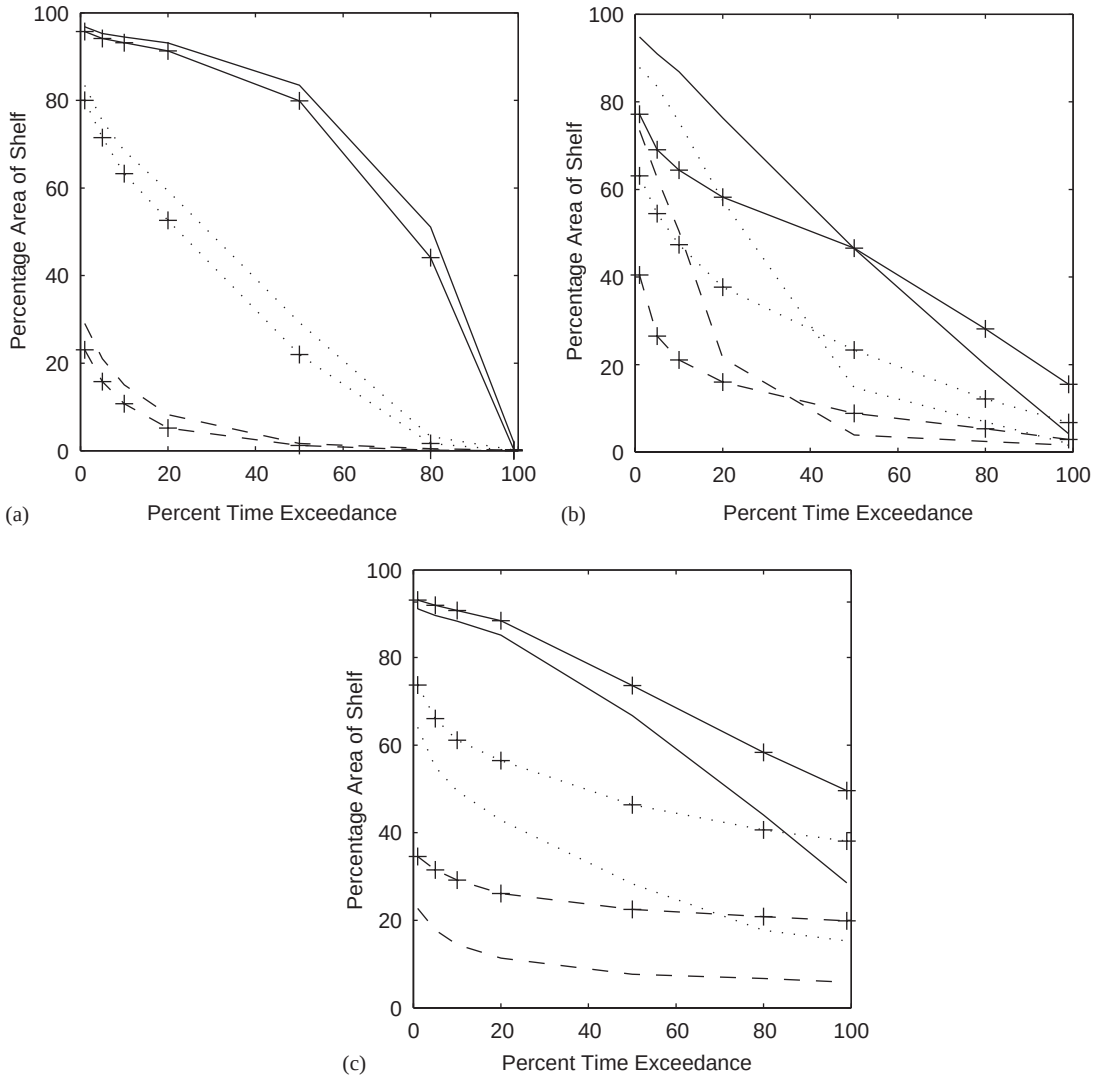

Fig. 8. Threshold exceedances for three different τ_{cr} values for (a) currents alone, (b) waves alone and (c) wave–current interactions for both the NW monsoon (no symbol) and the trades (+). Solid line: $\tau_{cr}=0.05\,\mathrm{N\,m^{-2}}$, dotted line: $\tau_{cr}=0.26\,\mathrm{N\,m^{-2}}$, dashed line: $\tau_{cr}=1.25\,\mathrm{N\,m^{-2}}$. Low τ_{cr} values correspond to fine, non-cohesive sediments, larger τ_{cr} values correspond to coarser non-cohesive sediments or fine cohesive sediments.

the Coral Sea, and extend into and through Torres Strait to the west.

During the NW monsoon (January–March), the sediment plume from the Fly River moves in two dominant directions following the mean flow (Fig. 7e). Assuming that 50% of the Fly River sediment is deposited directly offshore from the delta, 34% of the plume moves north-eastwards along the south coast of PNG, and then southwards past Port Moresby (Fig. 7c). Another significant portion of the plume (10%) moves southwards to the east of Cape York, inside the Northern Great Barrier Reef. Three percent of the plume heads westwards through Torres Strait, and the remaining 3% offshore to be deposited in the Coral Sea.

During the SE trades (April–June), the Fly River plume alters its path such that 24% of the sediment is distributed to the north-east along the south coast of PNG, 13% directly offshore to the Coral Sea, and 11% westwards into, and through Torres Strait. The remaining 2% travels southwards on the eastern side of Cape York (Fig. 7d). Wolanski et al. (1984) analysed LANDSAT and Coastal Zone Colour Scanner (CZCS) imagery, and their modelled trades plume indicates similar characteristics. The predicted sediment budget from this modelling study agrees with the preliminary budget proposed by Harris et al. (1993); however, a strong seasonal dependence is evident which was not apparent from the sediment facies models.

5.3. *Influence of waves on sediment movement in Torres Strait*

For sediment to be resuspended from the seabed, the bed shear stress must exceed some critical shear stress τ_{cr}, which is a function of grain size, density and shape, water density and viscosity and whether the sediment grains are cohesive or cemented. The model has been run for τ_{cr} values between 0.05 and 1.25, the lower value indicative of very fine (0.01 mm) non-cohesive sediments, and the upper value indicative of coarser (2 mm) non-cohesive sediment, and fine cohesive sediments with a medium to large bulk density (Madsen and Grant, 1976; Mitchener and Torfs, 1996). The shear stress was then determined for currents, waves alone, and due to wave–current-induced flows.

Wave-induced bottom shear stress is then calculated from bottom orbital velocity estimates using linear wave theory and equations of Jonsson (1966)

$$\tau_\omega = \rho C_D u_{b,max}^2.$$

Jonsson (1966) uses a value for the friction coefficient, C_D, of 0.0033. Wave–current interactions have also been considered. Wave data were interpolated onto the model grid using a $1/r$ nearest-neighbour interpolation. The iterative procedure of Madsen (1994) to determine u^*_{wc} was used. τ_{wc} was determined at six hourly intervals from output bottom currents and available wave data for the 3-month monsoon period (January–March) and the 3-month trades period (April–June). For each of τ_c, τ_w and τ_{wc} variables, the number of times the critical shear stress for a given grain size was exceeded at each bathymetric grid point was summed to derive a threshold exceedance map of the Torres Strait and Gulf of Papua region.

The surface areas of the shelf (defined as <300 m) where the relative bottom stress exceeded the critical shear stress for the three different critical shear stresses are displayed in Fig. 8. Note that the estimated areas are for assumed grain sizes and show only the possibility of mobilising a certain grain size if it were present at a given location on the shelf.

Fig. 8a indicates that tidal and wind-driven currents during both the monsoon and trades are capable of moving 0.01 mm diameter grain quartz over almost the entire shelf. These plots indicate that not all of the shelf will be resuspended at some point in time, and no part of the shelf will be resuspended the entire time. The similarity between the monsoon and trades threshold exceedances supports the suggestion that tidal currents dominate over wind-generated currents in the region.

A large seasonal variation in threshold exceedances due to waves in the model domain is predicted, indicated by Fig. 8b, as a result of increased wave activity in the Gulf of Papua during the SE trades season. During the monsoon, it is notable that almost 100% of the 0.01 mm sediment on the shelf is resuspended at some point in time. However, during the trades a large portion

is not moved at all, with only approximately 80% being resuspended at some point in time. During the monsoon, only a small portion (<5%) of the 0.01 mm sediment on the shelf is mobilised for the whole time; however during the trades a much larger portion (~15%) of the shelf moves the entire time. This pattern showing a seasonal crossover is repeated for each grain size distribution, clearly indicating the influence of the NGBR in sheltering the south-east trades wave activity from a large portion of the model domain. Hence during the trades, waves are capable of resuspending sediments in the Gulf of Papua only, but they tend to keep these sediments mobilised for a larger portion of time than observed during the monsoon (refer to Fig. 2 for seasonal wave activity).

Threshold exceedances due to wave–current-induced bed shear stress are the most realistic case, and are displayed in Fig. 8c. For 0.01 mm sediments during the SE trades, ~70% of the shelves sediments move at some stage during the 90-day model run, and ~55% of the shelf study area is resuspended for the entire period. These numbers both reduce to ~20% for the 2 mm sediment. This would suggest, shown by the near horizontal lines in Fig. 8c, that sediment moves either the entire time, or not at all, and hence that wave–current-induced bed stresses are more energetic than the oscillations in magnitudes of currents or waves alone. During the monsoon, similar areas are mobilized for some period, however, significantly less (25% and 5% for 0.01 and 2 mm (or cohesive), respectively) are mobilized for the entire monsoon period. Significantly more sediment is mobilised during the trades than the monsoon when wave–current interactions are considered due to increased wave activity during the trades, and mobilization increases markedly when wave–current interactions are considered compared to waves only, and currents only. Seasonal variation is observed for both fine and coarse grained sediment.

5.4. Classification of dominant processes

The large portions of shelf moved due to wave–current interaction poses the question as to whether the area is wave dominated, tidally dominated, or whether it is a truly mixed region.

Porter-Smith (2001) presents a classification scheme based on percent exceedances, where $t/w<1/3$ implies waves dominate, $t/w>3$ implies currents dominate, and $1/3<t/w<3$ implies a mixed area, where w is the % time of wave threshold exceedance and t is the % time of tidal current threshold exceedance. Maps of t/w for the NW monsoon and SE trades are shown in Figs. 9a, b and 10a, b, respectively. Figs. 9c, d and 10c, d show the fraction of time the sediment of each grain size is mobilized under combined wave–current conditions.

During the NW monsoon, fine sediment is largely tidally dominated in the deep water Gulf of Papua and amongst the Torres Strait Islands. A narrow band along the coast of Papua New Guinea in the Gulf of Papua is wave dominated, and the remaining large area indicates a mixed environment. With increasing grain size, the areas which are tidally dominated diminish to near zero for coarse (or cohesive) sediment where some small patches amongst the Torres Strait Islands are tidally dominated. For 0.01 and 2 mm sediment, the mixed area decreases as the wave-dominated areas increase, until for coarse sediment, the shelf is predominantly wave dominated with only small patches which are mixed or dominated by tides. The wave motion during the monsoon, although small, is the dominant mechanism for resuspending larger sediments. Regions of wave dominance are observed to be regions where sediments are mobilized for 100% of time for sediments with both high and low critical shear stresses (Fig. 9c and d).

During the trades, the map of t/w is very similar as for the monsoon for fine sediment. A larger area to the west of Torres Strait is tidally dominated as a result of the decreased wave activity in this region during the trades due to the shelter of the NGBR and Cape York. Mixed and tide-dominated areas decrease in magnitude, and the wave-dominated areas increase in magnitude, with increasing grain size. The trades show less variation with grain size than the monsoon. For sediments of greater critical shear stress during the trades, a large area within, west of Torres

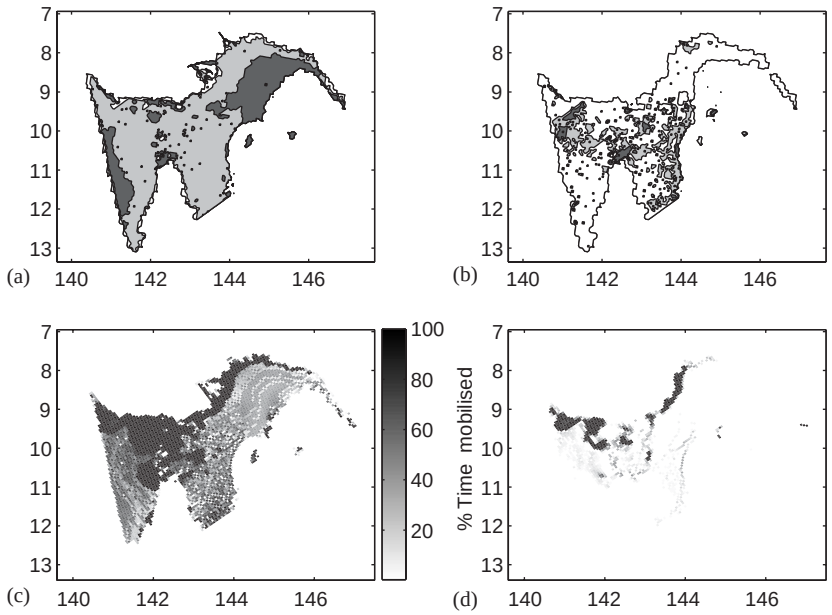

Fig. 9. NW monsoon classification for critical shear stress values of (a) $\tau_{cr} = 0.05\,\mathrm{N\,m^{-2}}$ and (b) $\tau_{cr} = 1.25\,\mathrm{N\,m^{-2}}$. Dark grey—tidal dominated, grey—mixed area, bounded white—wave dominated. Fraction of time sediment mobilized for (c) $\tau_{cr} = 0.05\,\mathrm{N\,m^{-2}}$ and (d) $\tau_{cr} = 1.25\,\mathrm{N\,m^{-2}}$ during the monsoon.

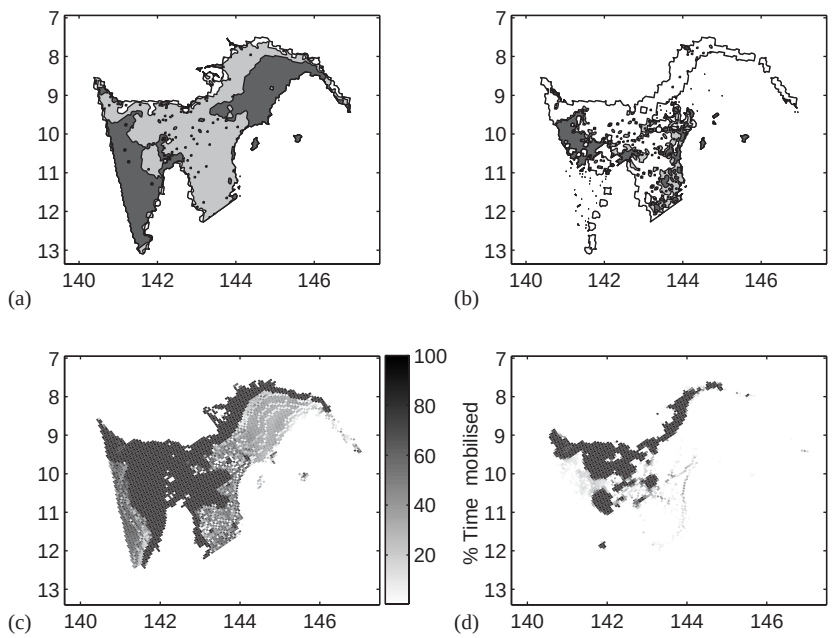

Fig. 10. SE trades classification for critical shear stress values of (a) $\tau_{cr} = 0.05\,\mathrm{N\,m^{-2}}$ and (b) $\tau_{cr} = 1.25\,\mathrm{N\,m^{-2}}$. Dark grey—tidal dominated, grey—mixed area, bounded white—wave dominated. Fraction of time sediment mobilized for (c) $\tau_{cr} = 0.05\,\mathrm{N\,m^{-2}}$ and (d) $\tau_{cr} = 1.25\,\mathrm{N\,m^{-2}}$ during the trades.

Strait and just inside the Great Barrier Reef are dominated by tides, whereas these same areas are mixed or wave dominated during the monsoon. This result is an indicator of the shelter of wave activity provided by the Northern Great Barrier Reef during the SE trades. The size of the wave dominated area in the Gulf of Papua is similar for each season.

6. Discussion

Although the interactions of waves and currents have been considered, several factors complicating the modelling of where mobilisation occurs have been ignored. Real shelf sediments are rarely cohesionless quartz spheroids, but a mixture of poorly sorted gravel, sand and mud, and are often transported across continental shelves to locations where they are in hydrodynamic equilibrium (Nittrouer and Wright, 1994). By assuming a constant grain size, areas of continuous mobilisation (100% exceedance) are most likely an overestimate.

The hydrodynamic model results are suitable for the purpose of investigating seasonal variation of the oceanic currents, capable of reproducing observed trends in the area. However, quantitatively, the model could be improved. An approach similar to that taken by Bode and Mason (1994) of specifying reef porosity may be valuable for improving quantitative comparisons in the future.

The estimate of current-induced shear stress ignores the frictional drag of bedforms (Davies, 1985). Large bedforms are found in Torres Strait (Harris, 1988), and where these occur, threshold exceedances will be overestimated. The estimate of wave, and wave–current, induced bed shear stress will likewise be hindered by the presence of bed ripples.

The wave data obtained from BoM are modelled using the WAM wave model. Although this model performs well in open water, the scale of the wave calculations and the physics of the model cannot account for the bathymetrically complex areas such as Torres Strait and the NGBR, where wave sheltering, refraction and reflection occur. Hence the wave induced, and the influence on the wave–current induced, 100% threshold exceedances within the domain are most likely also overestimated.

Resuspension of settled sediment is not included in the tracer model carried out in this study. Resuspension of material from the seabed would result in plumes of higher suspended sediment concentrations. As a result, the modelled sediment budget may be an underestimate in regions of greater mobility. Flocculation processes are also not included in the model. Flocculation will increase settling velocities such that the distance modelled plumes extend may be overestimated in areas where flocculation is important.

7. Summary

The study involved numerical modelling of the Torres Strait–Gulf of Papua region using a non-linear 3D hydrodynamic model. Realistic forcing was used to predict currents due to tides, atmospheric inputs and mean density induced flows, and despite complex bathymetry the model provided currents qualitatively consistent to those measured in the field. Additional current metre data for model validation are to be collected during 2004.

Tracers were input into the model to establish a sediment budget of the Fly River sediment plume. The predicted budget, during the monsoon, is consistent with the preliminary form proposed by Harris et al. (1993) based upon the sedimentology and morphology of the area. However, it is found that there is a strong seasonal dependence on the Fly River sediment budget. Increased sediment load is directed towards Torres Strait during the trade season, corresponding to periods of increased rainfall in the New Guinea highlands, and hence increased sediment load in the Fly River.

Harris et al. (1993) collected sediment cores from the Fly Delta which indicate seasonal sand–mud interbeds. In support of these results, predictions of sediment mobility due to wave–current interactions were found to alter significantly between the trades and monsoon seasons. Sediment was found to be mobilised over a larger

portion of the shelf in the Gulf of Papua during the Trade season.

Given the model constraints, we have identified the transport paths of mining waste derived from the Fly River, which pose a possible threat to the Torres Strait marine environment. The identification of a zone of possible increased bed shear stress on the NGBR has implications for the proposed emplacement of the Torres Strait pipeline, through increased scour along the line with the potential for environmental impact on the nearby coral reefs. Available data are unable to resolve many of the model predictions from this study. Further fieldwork is to be carried out during 2004 for this zone, to determine whether or not such processes are actually occurring in this area.

Acknowledgements

The authors are grateful to CSIRO Marine Research for provision of MECO and to the National Tidal Facility for the provision of tidal data from tidal stations in the area of study. Thanks to J. Dunn of CSIRO Marine Research for provision of the CARS data, D. Greenslade of the Bureau of Meteorology for provision of the WAM wave data and Michael Hughes for valuable discussion. We also acknowledge the input of four anonymous reviewers.

References

Alongi, D.M., Christoffersen, P., Tirendi, F., Robertson, A.I., 1992. The influence of freshwater and material export on sedimentary facies and benthic processes within the Fly Delta and adjacent Gulf of Papua (Papua New Guinea). Continental Shelf Research 12 (2), 287–326.

Amin, M., 1978. A Statistical Analysis of Storm Surges in Torres Strait. Austalian Journal of Marine and Freshwater Research 29, 479–496.

Andrewartha, J.R., Walker, S.J., 1997. Boags rocks environmental impact assessment program task 6.4: Hydrodynamic modeling study, preliminary report, Technical Report No. OMR-96/107, CSIRO Division of Marine Research.

Andrewartha, J.R., Walker, S.J., 1999. North west shelf modelling project preliminary report. Technical Report No. OMR-123/122, CSIRO Marine Research.

Blumberg, A.F., Herring, J., 1987. Circulation modelling using orthogonal curvilinear coordinates. In: Nihoul, Jamart (Eds.), Three-dimensional Models Of Marine And Estuarine Dynamics. Elsevier, Amsterdam.

Bode, L., Mason, L.B., 1994. Tidal modeling in Torres Strait and the Gulf of Papua. In: Choat, J.H., Bellwood, O., Saxena, N. (Eds.), Recent Advances in Marine Science and Technology, 95, Proceedings of the PACON Symposium (July 1994). Townsville, Australia, pp. 55–65.

Bowden, F., Hamilton, P., 1975. Some experiments with a numerical model of circulation and mixing in a tidal estuary. Estuarine and coastal Marine Science 3, 281–301.

Csanady, G., 1982. Circulation in the Coastal Ocean. D. Riedel Publishing company, Dordrecht.

Davies, A., 1985. Field observations of the threshold of sediment motion by wave action. Sedimentology 32, 685–704.

Dyer, K., 1986. Coastal and Estuarine Sediment Dynamics. Wiley, New York.

Flater, D., 1999. Harmonic tide clock and tide calculator. WWW page: http://www.flaterco.com/xtide.

Greenslade, D., 2001. Personal Communication. Bureau of Meteorology.

Harris, P.T., 1988. Sediments, bedforms and bedload transport pathways on the continental shelf adjacent to Torres Strait, Australia-Papua New Guinea. Continental Shelf Research 8 (8), 979–1003.

Harris, P.T., 1989. Sandwave movement under tidal and wind-driven currents in a shallow marine environment: Adolphus Channel, northeastern Australia. Continental Shelf Research 9, 981–1002.

Harris, P.T., 1991. Reversal of subtidal dune asymmetries caused by seasonally reversing wind-driven currents in Torres Strait, northeastern Australia. Continental Shelf Research 11 (7), 655–662.

Harris, P.T., 1993. Near-bed current measurements from Torres Strait obtained during Jan–Mar 1993 aboard RV Southern Surveyor. Technical Report 29. Ocean Sciences Institute, University of Sydney.

Harris, P.T., 1994a. Comparison of tropical, cabonate and temperate, siliclastic tidally dominated sedimentary deposits: Examples from the Australian Continental Shelf. Australian Journal of Earth Sciences 41, 241–254.

Harris, P.T., 1994b. Muddy Waters: The physical Sedimentology of Torres Strait. In: Choat, J.H., Bellwood, O., Saxena, N. (Eds.), (Ed), Recent Advances in Marine Science and Technology, 95, Proceedings of the PACON Symposium (July 1994). Townsville, Australia, pp. 149–160.

Harris, P.T., 1999. Environmental management of Torres Strait: A Marine Geologist's perspective. In: Gostin, V.A. (Ed), Gondwana to Greenhouse: Environmental Geoscience—an Australian perspective. pp. 149–160.

Harris, P.T., Baker, E., 1991. The nature of sediments forming the Torres Strait turbidity maximum. Australian Journal of Earth Sciences 38, 65–78.

Harris, P.T., Baker, E., Cole, A., Short, S., 1993. A preliminary study of sedimentation in the tidally dominated Fly River Delta, Gulf of Papua. Continental Shelf Research 13 (4), 441–472.

Johnson, M.A., Kenyon, N.H., Belderson, R.H., Stride, A.H., 1982. Sand transport. In: Stride, A.H. (Ed.), Offshore tidal sands: process and product. Chapman & Hall, London, pp. 58–94.

Jonsson, I., 1966. Wave boundary layers and friction factors. In: Proceedings of the 10th Conference on Coastal Engineering, vol. 1. ASCE, Tokyo, pp. 127–148.

Kalnay, E., Kanamitsu, M., Kistler, R., Collins, W., Deaven, D., Gandin, L., Iredell, M., Saha, S., White, G., Woollen, J., Zhu, Y., Chelliah, M., Ebisuzaki, W., Higgins, W., Janowiak, J., Mo, K.C., Ropelewski, C., Wang, J., Leetma, A., Reynolds, R., Jenne, R., Joseph, D., 1996. The NCEP/NCAR 40-year reanalysis project. Bulletin of the American Meteorological Society 77 (3), 437–471.

Large, W., Pond, S., 1981. Open ocean momentum flux measurements in moderate to strong winds. Journal of Physical Oceanography 11, 324–336.

Madsen, O., 1994. Spectral wave–current bottom boundary layer flows. In: Proceedings of the 24th International Conference on Coastal Engineering. ASCE, Kobe. pp. 384–398.

Madsen, O., Grant, W., 1976. Quantitative description of sediment transport by waves. In: Proceedings of the 15th International Conference on Coastal Engineering, vol. 2. ASCE, pp. 1093–1112.

McMillan, J., 1982. A Global Atlas of GEOS-3 Significant Wave height Data and Comparison of the Data with National Buoy Data (156882). Technical report, NASA, Wallops Flight Centre, Virginia.

Melville, W., Buchwald, V., 1976. Oscillations of the Gulf of Carpentaria. Journal of Physical Oceanography 4, 83–90.

Mesinger, F., Arakawa, A., 1976. Numerical Methods used in atmospheric models. Technical Report. World Meteorological Organisation.

Mitchener, H., Torfs, H., 1996. Erosion of mud/sand mixtures. Coastal Engineering 29, 1–25.

Nittrouer, C., Wright, L., 1994. Transport of particles across continental shelves. Reviews of Geophysics 32 (1), 85–113.

NOAA, 1988. NGDC. Data Announcement 88-mgg-02, digital relief of the surface of the earth. ETOPO-5. WWW Page: http://www.ngdc.noaa.gov/mgg/global/etopo5.html.

Porter-Smith, R., 2001. Personal Communication. Geoscience Australia. Hobart, Tasmania.

Ridgway, K.R., Dunn, J.R., Wilkin, J.L., 2000. A climatology of the waters around Australasia using 4-dimensional weighted least squares fitting. Technical Report, CSIRO Marine Research.

Stride, A.H., 1982. Offshore Tidal Sands: Process and Product. Chapman and Hall, London.

Walker, S.J., 1996. Hydrodynamic model of Port Phillip Bay. Technical Report 38, CSIRO Port Phillip Bay Environmental Study.

Walker, S.J., 1999. Coupled hydrodynamic and transport models of Port Phillip Bay, a semi-enclosed bay in south-eastern Australia. Marine Freshwater Research 50, 469–481.

Walker, S.J., Fandry, C., 1993. Modelling effluent dispersal in Australian coastal waters—Devonport 1991–1992, hydrodynamic modeling. Technical Report No. OMR-59/40, CSIRO Division of Oceanography.

Walker, S.J., Waring, J., 1998. MECO Technical Report No. OMR-118/120, CSIRO Marine Research.

Wessell, P., Smith, W., 1996. A global self-consistent, hierarchial, high resolution shoreline database. Journal of Geophysical Research 101, 8741–8743.

Wolanski, E., 1986. The physical oceanography of Torres Strait. In: Haines, A., Williams, G.C., Coates, D. (Eds.), Torres Strait Fisheries Seminar. Australian Govt. Publ. Service, pp. 275–291.

Wolanski, E., Eagle, M., 1991. Oceanography and fine sediment transport, Fly River Estuary and Gulf of Papua. Coastal Engineering—Climate for Change. 10th Australasian Conference on Coastal and Ocean Engineering, Auckland, 2–6 December 1991, pp. 453–457.

Wolanski, E., Pickard, G., Jupp, D., 1984. River plumes, coral reefs and mixing in the Gulf of Papua and the northern Great Barrier Reef. Estuarine Coastal and Shelf Science 18, 291–314.

Wolanski, E., Thomson, R., 1984. Wind-driven circulation on the Northern Great Barrier Reef continental shelf in summer. Estuarine Coastal and Shelf Science 18, 271–289.

Wolanski, E., Ridd, P., Inoue, M., 1988. Currents through Torres Strait. Journal of Physical Oceanography 18, 1535–1545.